Available online at www.sciencedirect.com

SCIENCE DIRECT®

Magnetic Resonance Imaging 23 (2005) 711–722

MAGNETIC RESONANCE IMAGING

Application of phase consistency to improve time efficiency and image quality in dual echo black-blood carotid angiography

Eugene G. Kholmovski*, Dennis L. Parker

Department of Radiology, Utah Center for Advanced Imaging Research, University of Utah, Salt Lake City, UT 84132, USA

Received 1 March 2005; accepted 23 May 2005

Abstract

There is a considerable similarity between proton density-weighted (PDw) and T2-weighted (T2w) images acquired by dual echo fast spin-echo (FSE) sequences. The similarity manifests itself not only in image space as correspondence between intensities of PDw and T2w images, but also in phase space as consistency between phases of PDw and T2w images. Methods for improving the imaging efficiency and image quality of dual echo FSE sequences based on this feature have been developed. The total scan time of dual echo FSE acquisition may be reduced by as much as 25% by incorporating an estimate of the image phase from a fully sampled PDw image when reconstructing partially sampled T2w images. The quality of T2w images acquired using phased array coils may be significantly improved by using the developed noise reduction reconstruction scheme, which is based on the correspondence between the PDw and T2w image intensities and the consistency between the PDw and T2w image phases. Studies of phantom and human subject MRI data were performed to evaluate the effectiveness of the techniques.

Keywords: Magnetic resonance imaging; Fast spin-echo; Phase consistency; Reconstruction technique; POCS

1. Introduction

High-resolution magnetic resonance angiography (MRA) has significant potential for improving noninvasive imaging of blood vessels and enabling better assessment of the degree and nature of vascular disease. Black-blood MRA techniques [1–8], in which the signal from flowing blood is suppressed while strong signals from surrounding static tissues are maintained, has been shown to provide excellent depiction of both lumen and outer wall boundary of blood vessels. The quality of black-blood techniques depends upon how effectively the blood signal can be suppressed so that it does not contribute confounding signals to the vessel wall images. Blood suppression in black-blood imaging was improved with the introduction of selective preinversion pulses [1,2] that cause the spins outside of the imaged slice to be inverted while the spins within the slice are unaffected. This selective inversion is usually accomplished by a nonselective inversion of the entire volume followed by a selective inversion of the imaged slice. The time between inversion and image acquisition is selected based upon the time required to null the signal from the blood. Blood that flows into the imaged slice does not produce any MR signals; therefore, the contrast between stationary tissue and flowing blood is very high.

Double inversion fast spin-echo (FSE) techniques [3–8] work very well for suppressing the majority of blood signal, thereby providing excellent contrast between vessel wall and blood in black-blood carotid angiography. Unfortunately, there may be some flow profiles or imaging planes where blood remains within the slice between the inversion pulse and the time of imaging. Such blood retains a bright signal, which can easily be confused with tissue signal. Acquisition of images at two echo times, a proton density-weighted (PDw) and a T2-weighted (T2w) image, can assist in the discrimination between blood and atherosclerotic plaque due to the significant difference in their T2 relaxation times and also in the identification of plague components [9–11].

Dual echo (dual contrast) FSE sequences are widely used to simultaneously acquire high-resolution PDw and T2w images. In typical dual echo FSE imaging, the first half of the echo train is used to acquire PDw k-space data, and the second half is used to acquire T2w data [12,13]. The

* Corresponding author. Tel.: +1 801 585 1755; fax: +1 801 585 3592.
E-mail address: ekhoumov@ucair.med.utah.edu (E.G. Kholmovski).

0730-725X/$ – see front matter © 2005 Elsevier Inc. All rights reserved.
doi:10.1016/j.mri.2005.05.002

effective echo time (TE) for each image is determined by the echo time of the echoes, which are used to acquire the central (low frequency) part of the corresponding k-space. Proton density-weighted and T2w images acquired by such a way implemented dual echo FSE sequence are perfectly spatially coregistrated, which greatly simplifies their analysis and postprocessing.

The main disadvantages of dual echo FSE acquisition are the increased scan time, in comparison with single echo acquisition, and the low SNR of the T2w images. Well-known method to improve time efficiency of dual echo FSE imaging is echo-sharing technique [14,15]. Imaging efficiency improvement is achieved by the use of the same high frequency k-space data in both images. Primary disadvantage of this technique is a mixed contrast of the images due to inclusion of longer TE echoes in the PDw image and shorter TE echoes in the T2w image. This effect becomes crucial when not only PDw and T2w images but also their ratio contains important diagnostic information. Black-blood carotid angiography is one of such cases when it is preferably to acquire images with the true PDw and T2w contrast.

The PDw and T2w images acquired by dual echo FSE pulse sequence have a considerable similarity in image intensity and phase distributions. The goal of this work is to use this redundant information to improve the imaging efficiency and image quality of dual echo black-blood carotid angiography.

2. Materials and methods

The PDw and T2w images acquired by the dual echo FSE sequence can be described by the following equations:

$$I^{PD}(r) = I(r)S(r)\Phi^{PD}(r) + N^{PD}(r) = J^{PD}(r) + N^{PD}(r) \quad (1)$$

$$I^{T2}(r) = I(r)W(r)S(r)\Phi^{T2}(r) + N^{T2}(r) \quad (2)$$

where $I(r)$ is the proton density magnetization magnitude (real nonnegative function); $S(r)$ is the magnitude of the coil sensitivity (real positive definite and smoothly varying function); $J^{\mathrm{PD}}(r)$ is the noise-free PDw image; $\Phi^{\mathrm{PD}}(r)$ and $\Phi^{\mathrm{T2}}(r)$ are the phase variation factors in noise-free PDw and T2w images; $W(r)$ is the T2 weighting factor (real positive definite function); and $N^{\mathrm{PD}}(r)$ and $N^{\mathrm{T2}}(r)$ are complex noise contributions in the PDw and T2w images. The noise in the corresponding PDw and T2w images can be assumed to be uncorrelated. The real and imaginary components of $N^{\mathrm{PD}}(r)$ and $N^{\mathrm{T2}}(r)$ may be characterized by zero mean Gaussian probability density functions with the same standard deviation and can also be considered mutually uncorrelated.

Eqs. (1) and (2) show that the differences between noise-free PDw and T2w images may be characterized by T2 weighting and phase variation factors. The T2 weighting factor, $W(r)$, characterizes the changes in intensity between noise-free PDw and T2w images and can be defined by the following equation:

$$W(r) = \exp\left(\frac{TE^{PD} - TE^{T2}}{\tilde{T}2(r)}\right) \quad (3)$$

where $\mathrm{TE}^{\mathrm{PD}}$ and $\mathrm{TE}^{\mathrm{T2}}$ are the effective echo times of the PDw and T2w images, and $\tilde{\mathrm{T}}2$ is an apparent spin-spin (transverse) relaxation time for the given tissue and given dual echo FSE sequence. It is reasonable to assume that the range of possible values of $W(r)$ is limited: $W(r)\in[0,\beta]$. The upper bound, β, may easily be determined if $\mathrm{TE}^{\mathrm{PD}}$ and $\mathrm{TE}^{\mathrm{T2}}$ of the dual echo FSE acquisition and apparent spin-spin relaxation times of imaged tissues are known. For the majority of tissues, $\tilde{\mathrm{T}}2$ is close to the true tissue spin-spin relaxation time T2. However, for some tissues, there is a considerable discrepancy between T2 and $\tilde{\mathrm{T}}2$. The apparent spin-spin relaxation time in J-coupled systems such as lipids depends not only on the physical properties of the tissue but also the number and rate of refocusing RF pulses in the FSE sequence used to acquire the image [16,17]. In FSE acquisitions, the MR signal in J-coupled tissues for a fixed TE may be increased by increasing the number of refocusing RF pulses and decreasing the echo spacing time. This outcome should be taken into account when calculating the upper bound of the range of the T2 weighting factor for the given FSE acquisition.

Phase variation factors $\Phi^{\mathrm{PD}}(r)$ and $\Phi^{\mathrm{T2}}(r)$ are defined by $\Phi^{\mathrm{PD}}(r)=\exp[i\phi^{\mathrm{PD}}(r)]$ and $\Phi^{\mathrm{T2}}(r)=\exp[i\phi^{\mathrm{T2}}(r)]$, where $\phi^{\mathrm{PD}}(r)$ and $\phi^{\mathrm{T2}}(r)$ are the spatially dependent phases of the noise-free PDw and T2w images. In an ideal case, the images reconstructed from MR data should be real. However, images acquired by an actual MRI system are complex due to incidental phase variations that occur due to various factors such as a noncentered sampling window, patient-to-patient variations in coil loading, RF angle inhomogeneity, eddy currents induced by the gradients, B_0 field inhomogeneities, susceptibility and chemical shift effects. The first of these factors tends to create global, slowly varying phase variations, while the last three are responsible for local, rapidly changing phase variations. In the case of the FSE sequences, the latter factors (B_0 field inhomogeneities, susceptibility and chemical shift effects) are suppressed, and the remaining phase variation may be described by a slowly varying function.

One of the main requirements for obtaining high-quality MR images using an FSE sequence is stability of the phase variations during the data acquisition: The image phase distribution (neglecting phase encoding) must be the same for all echo trains and all echoes that compose each echo train. In cases where this condition is not met, the acquired images suffer from considerable ghosting artifacts. In this work, we assume that the required phase variation stability during dual echo FSE acquisition is achieved. Therefore, the phase variations in the PDw and T2w images acquired

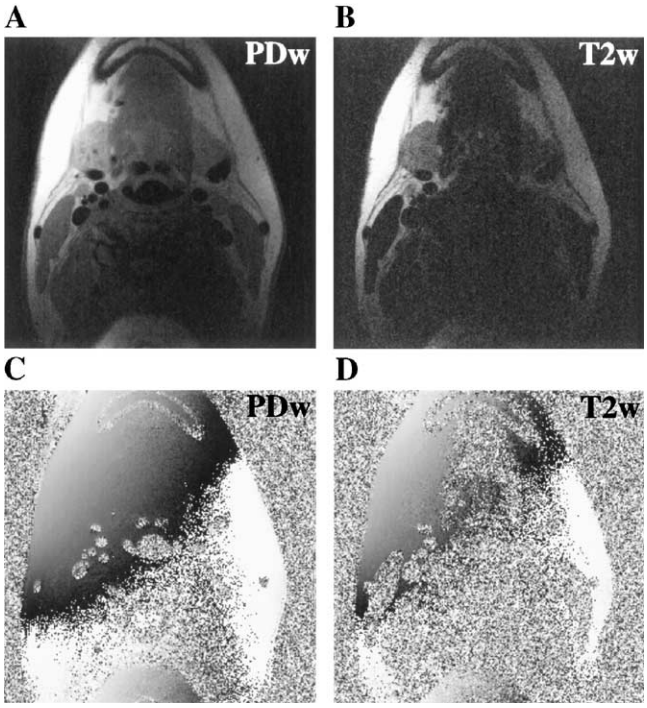

Fig. 1. Typical PDw and T2w magnitude (A, B) and phase (C, D) images in the case of dual echo, double inversion black-blood carotid angiography. Individual coil images are presented. The phases are comparable in high SNR areas of the PDw and T2w images. Considerable discrepancies between phases of the PDw and T2w images are obvious in the background and areas of low SNR. For many low SNR areas of the T2w image, the corresponding PDw image has considerably higher SNR, allowing a more accurate estimate of the true image phase.

using the dual echo FSE sequence should be the same: $\Phi(r)=\Phi^{\mathrm{PD}}(r)=\Phi^{\mathrm{T2}}(r)$. This observation will be referred to as phase consistency in this paper.

2.1. Improvement of time efficiency

To reduce scan time, a partial k-space acquisition and reconstruction method such as those described by Margosian et al. [18] and Cuppen and van Est [19], homodyne detection [20] or projection onto convex sets (POCS) [21–23] may be used. The quality of a partial k-space acquired image depends strongly on the phase estimation used as a constraint for reconstruction from undersampled k-space data [23,24]. If the exact phase is available as a constraint, the complete k-space data set may be recovered. Usually, the phase estimation is generated from the central part of the acquired k-space. This low-resolution phase estimation may degrade the quality of the final image if there are any inconsistencies between the true image phase and its estimation. To improve the quality of the final image, low undersampling rates with improved phase estimation should be used. There is an obvious trade-off between the achievable undersampling rate and the quality of the reconstructed image.

An additional requirement for obtaining a high-quality image from partial k-space data is to have high SNR in the phase estimation. When the phase estimate is calculated from the low frequency part of acquired k-space data, this requirement is partially met. However, the noise in this phase estimation to be used as a reconstruction constraint is highly correlated with the noise in the k-space data used to find the final image. The ideal reconstruction phase constraint should have high SNR and be completely uncorrelated with noise in k-space data used to obtain the final image. To find such a phase constraint, the acquisition of an additional reference image, with the same phase variations as in the partial acquired image, is required. The reference scan method of finding phase estimate is not often used because of the significant decrease in time efficiency of an acquisition. However, the method has been successfully utilized for myocardium viability imaging [25].

It was established that the phase variations in the PDw and T2w images acquired by the dual echo FSE sequence are the same even though the image contrast is significantly different (see Fig. 1). Therefore, one of the two echo time images may be obtained with greatly reduced k-space coverage by incorporating an estimate of the image phase from the fully sampled image when reconstructing the undersampled image. In this manner, the total scan time for dual echo acquisition might be reduced by as much as 25%, and the resulting undersampled images might be reconstructed without artifacts caused by incorrect phase estimations. As a rule, it is preferable to use a phase estimate from the PDw image to reconstruct the T2w image because of the significantly higher SNR of the PDw image.

The following method for improving imaging efficiency of dual echo black-blood carotid angiography has been developed:

1. Acquisition of a full k-space for PDw images and a fraction of k-space for T2w images;
2. Fourier reconstruction of the PDw image and the POCS-based reconstruction of the T2w image using the phase of the corresponding PDw image and the acquired T2w image k-space data as reconstruction constraints. A detailed description of the reconstruction algorithm is given below.

Let $\mathcal{K}$ be a set of k-space positions corresponding to the sampling on the Cartesian grid that gives the desired field of view (FOV) and resolution of the PDw and T2w images. $\mathcal{K}^{T2}$ is a subset of $\mathcal{K}$ that corresponds to the k-space positions of the acquired T2w image k-space data $K^{\mathrm{T2}}(k)$. Denoting Ω_1 to be the convex set of images whose phase is the same as the PDw image phase $\phi=\phi^{\mathrm{PD}}(r)$ and Ω_2 to be the convex set of images whose k-spaces agree with the acquired T2w image k-space data, we define the following projection operators onto Ω_1 and Ω_2:

$$P_1 : P_1(\phi)I_n = |I_n|e^{i\phi} \tag{4}$$

$$P_2 : P_2 I_n = F^{-1}\{\mathcal{R}\cdot\mathcal{F}\{I_n\}\} = \mathcal{F}^{-1}\{\mathcal{R}\cdot K_n\} \tag{5}$$

where $I_n = I_n^{T2}(r)$ is the T2w image after the nth iteration, of I_n, I_n^* denotes the complex conjugate of I_n, $\mathcal{F}$ and $\mathcal{F}^{-1}$ are the forward and inverse Fourier transform, $K_n = K_n(k)$ is the Fourier transform of I_n, and $\mathcal{R}$ is the data replacement operator defined as

$$\mathcal{R} \cdot K_n(k) = \begin{cases} K^{T2}(k), & k \in \mathcal{K}^{T2} \\ K_n(k), & k \notin \mathcal{K}^{T2} \end{cases} \text{with } k \in \mathcal{K} \tag{6}$$

The developed reconstruction algorithm consists of the following steps:

1. Reconstruct the PDw image and calculate the image phase to be used as a phase constraint ϕ.

2. Define the initial estimate: $I_0 = \mathcal{F}^{-1}\{K_0(k)\}$, where

$$K_0(k) = \begin{cases} K^{T2}(k), & k \in \mathcal{K}^{T2} \\ \gamma K^{PD}(k), & k \notin \mathcal{K}^{T2} \end{cases} \text{with } k \in \mathcal{K} \tag{7}$$

$K^{\mathrm{PD}}(k)$ are the acquired PDw image k-space data. The parameter γ is a correction factor that compensates for the difference between amplitudes of the PDw and T2w image k-space data. The factor may be calculated as a mean value of a ratio between the magnitudes of the central values of the T2w and PDw image k-space data. The initial estimate based on the combined k-space data (Eq. (7)) will have a mixed PD–T2w contrast. However, the contrast of the resulting image obtained after a few POCS iterations will correspond to the true T2w contrast. The initial estimate may also be found using only the acquired T2w data ($\gamma = 0$). However, the convergence of POCS algorithm with this initial estimate is, as a rule, suboptimal in comparison with the convergence of POCS algorithm with the initial estimate based on the combined k-space data.

3. Reconstruct the T2w image using POCS iterations: $I_n = P_2 P_1 I_{n-1}$, with $n \geq 1$. In most cases, convergence was achieved after only three to five iterations. Additional constraints such as image support or maximum of reconstructed image intensity may be easily incorporated into the reconstruction scheme.

The proposed algorithm is based on the POCS technique for reconstruction from undersampled k-space data [21–24]. The main distinctions between our method and the standard technique are the use of combined T2w and PDw image k-space data to calculate the initial image estimate and the use of the PDw image phase instead of the low-resolution phase estimate calculated from the central part of the T2w image k-space data. These changes from the standard algorithm result in improved algorithm convergence and considerable decrease in artifacts caused by incorrect phase estimation. An additional advantage of the proposed scheme is the potential to reconstruct high-quality T2w images from fewer total (more highly undersampled) k-space data (half of k-space data plus a few more lines) than is possible in the case of standard POCS reconstruction. This higher undersampling is achievable for the proposed reconstruction scheme because the phase of the PDw image is used as a reconstruction constraint instead of the low-resolution estimate calculated from the central part of the T2w image k-space. Hence, the trade-off between the undersampling rate and the quality of the reconstructed image may be bypassed in cases of dual echo FSE acquisition.

2.2. Noise reduction

Images reconstructed using partial Fourier reconstruction algorithms (homodyne detection, Cuppen and POCS) from undersampled k-space data have reduced SNR [23,26]. This effect further reduces the already intrinsically low SNR of T2w images, such as in the case of black-blood carotid angiography. The use of phased array coils can partially reduce this problem by distributing the high SNR performance of individual coil elements over the full-imaged FOV. However, the images reconstructed from the data acquired by phased array coils have increased noise bias in low-intensity areas of the reconstructed image [27]. In the majority of MRI studies, this effect is completely acceptable. Nevertheless, in the case of black-blood angiography, low-intensity image areas correspond not only to image background but also to vessel lumens, which are of primary diagnostic interest.

A noise reduction reconstruction (NRR) method for T2w images acquired by dual echo sequences using phased array coils has been developed. The method, which is based on the expected limitations on the T2 weighting factor and the phase consistency between PDw and T2w images, consists of three main steps: (1) calculation of the T2 weighting factor, $W(r)$; (2) identification and correction of pixels with high noise contribution; and (3) improvement of the reconstruction scheme for multicoil acquisition.

2.2.1. Calculation of T2 weighting factor, W(r)

An estimate of $W(r)$ may be calculated as the ratio between the resulting T2w and PDw images. To find the resulting T2w and PDw images, the standard sum-of-squares (SoS) reconstruction scheme [28] may be used:

$$I_{\mathrm{SoS}}(r) = \sqrt{\sum_{i=1}^{N} |I_i(r)|^2} \tag{8}$$

where N is the number of coils and $I_i(r)$ is the ith coil image. However, the estimate of the T2 weighting factor based on SoS-reconstructed PDw and T2w images deviates from the true value due to the noise bias in SoS-reconstructed images [27]. The deviations are especially strong in low SNR image areas and increase with the number of coils used to acquire the image.

To reduce this noise bias, a modification of the SoS reconstruction scheme (MSoS) has been developed. This method uses the properties of the Rician distribution, which describes the statistics of magnitude-reconstructed MR images [29,30], to significantly decrease the noise bias. The proposed reconstruction scheme is a generalization of

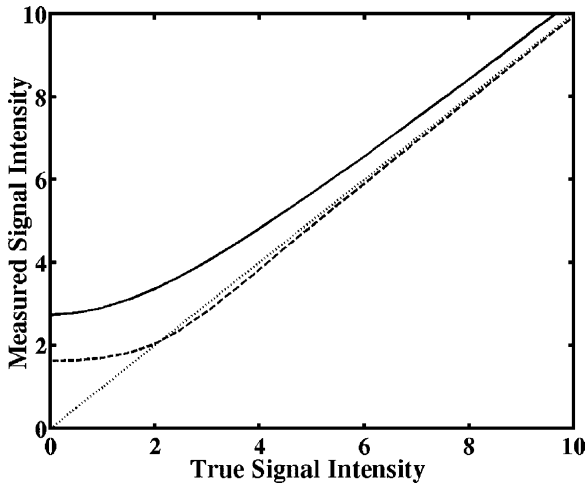

Fig. 2. The mean value of signal reconstructed from four individual coil images using SoS (solid line) and MSoS (dashed line) reconstruction schemes. The true value is plotted as a dotted line. The intensity is measured as units of noise standard deviation.

the image intensity correction scheme [31,32] for the case of multicoil image reconstruction and is given by

$$I_u^2(r) = \sum_{i=1}^{N} |I_i(r)|^2 - 2\sigma^2(I_i) \tag{9}$$

where $2\sigma^2(I)$ is the noise bias in the magnitude squared image $|I(r)|^2$. The noise bias may be calculated as a mean value of the air background in the magnitude squared image [27,29–32]. Finally, the resulting image is calculated using the following relationship:

$$I_{\mathrm{MSoS}}(r) = \begin{cases} I_u(r), & I_u^2(r) > 0 \\ 0, & I_u^2(r) \le 0 \end{cases} \tag{10}$$

Fig. 2 demonstrates that images reconstructed using the proposed modification of the SoS algorithm should have significantly smaller bias than images reconstructed using the standard SoS method. Therefore, the estimate of the T2 weighting factor based on the resulting PDw and T2w images reconstructed by Eq. (10) should have reduced systematic error and is given by

$$W(r) = \frac{I_{MSoS}^{T2}(r)}{I_{MSoS}^{PD}(r)} \tag{11}$$

$W(r)$ is equal to zero when $I_{\mathrm{MSoS}}^{\mathrm{PD}}(r)=0$. The calculated estimate of the T2 weighting factor, $W(r)$, is postprocessed as follows:

$$W_e(r) = \begin{cases} W(r), & W(r) < \beta \\ \beta, & W(r) \ge \beta \end{cases} \tag{12}$$

to satisfy the property of the ideal (noise-free) T2 weighting factor, $W(r) \in [0,\beta]$. In the case of dual echo FSE black-blood carotid angiography, we found that $\beta=1$ is a reasonable choice.

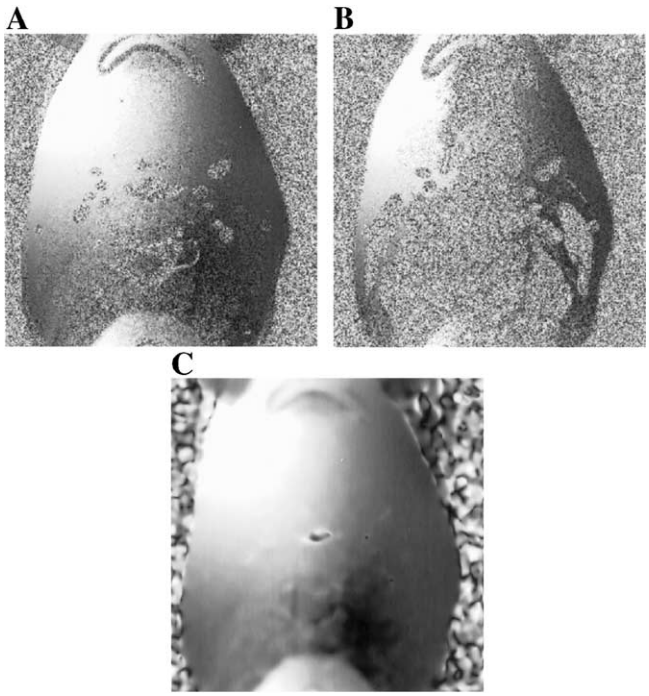

Fig. 3. The magnitude of the coil weighting factor calculated using Eq. (16) and (A) the original (high resolution) PDw image, (B) the original T2w image and (C) the low-resolution PDw image. The coil weighting factors are comparable in the high SNR areas of the PDw and T2w images. Considerable discrepancies between the coil weighting factors are obvious in the background and low SNR areas. In particular, the vessel lumen pixels have random coil weighting factor values in both A and B. However, the vessel lumen coil weighting factors are consistent with the coil weighting factor of the surrounding tissue pixels in the case of C.

2.2.2. Identification and correction of pixels with high noise contribution

This step of the NRR scheme should be implemented for individual coil T2w images. Eq. (2) may be rewritten as follows for the individual coil image:

$$I_i^{T2}(r) = J_i^{PD}(r)W(r) + N_i^{T2}(r) \tag{13}$$

Because of the range of the T2 weighting factor ($W(r)\in[0,\beta]$), the noise-free T2w image intensity should be lower than the product of β and the noise-free PDw image intensity. Pixels for which the condition is violated may be identified as those pixels with high noise contributions. Such pixels may be postprocessed in the following way to improve SNR:

$$I_i^{T2}(r) = \begin{cases} I_i^{T2}(r), & \beta|I_i^{PD}(r)| \geq |I_i^{T2}(r)| \\ W_e(r)I_i^{PD}(r), & \beta|I_i^{PD}(r)| < |I_i^{T2}(r)| \end{cases} \tag{14}$$

This step affects mainly pixels with no, or extremely low, MR signals (air background, vessel lumens in case of black-blood angiography and so on), as well as pixels in image areas where coils have low sensitivity.

2.2.3. Improved reconstruction scheme for multicoil acquisition

When k-space data are acquired by phased array coils, the resulting image is reconstructed as a combination of complex individual coil images:

$$I(r) = \sum_{i=1}^{N} \alpha_i(r) I_i(r) \tag{15}$$

where N is the number of coils, $I_i(r)$ is the ith coil image and $\alpha_i(r)$ is the coil weighting factor for the ith coil image. The standard SoS reconstruction scheme (Eq. (8)) is converted to this form using the following substitution:

$$\alpha_i(r) = I_i{}^*(r)/I(r) \tag{16}$$

In the noise-free case, Eq. (16) is given by

$$\alpha_i(r) = \frac{S_i(r)\Phi_i{}^*(r)}{\sqrt{\sum_{i=1}^{N} S_i^2(r)}} \tag{17}$$

Thus, the coil weighting factor, $\alpha_i(r)$, is an estimate of the product of the ith coil sensitivity and the phase variation factor weighted by the square root of the sum of the squares of the coil sensitivities. In the case of dual echo acquisition, the estimate of the coil weighting factor, $\alpha_i(r)$, may be calculated using PDw or T2w images. However, the estimate of the coil weighting factor based on PDw images should be much closer to the true (noise-free) value of $\alpha_i(r)$ than the estimate of the coil weighting factor based on the corresponding T2w images because of the considerably higher SNR of the PDw image (see Fig. 3). Therefore, the quality of the resulting T2w image may be improved if the image is reconstructed using the estimate of the coil weighting factors $\alpha_i(r)$ based on the corresponding PDw images:

$$I^{T2}(r) = \sum_{i=1}^{N} \alpha_i^{PD}(r) I_i^{T2}(r) \tag{18}$$

where $\alpha_i^{\mathrm{PD}}(r)$ is the coil weighting factor calculated from the PDw images using Eq. (16). Additional improvement may be achieved if the estimates of the coil weighting factors are calculated from low-resolution SoS and individual PDw coil images [33] or postprocessed by filtering or polynomial surface fit [24,34] using the fact that both coil sensitivities and phase variation factors may be described by smoothly varying functions. The postprocessed or low-resolution estimates of the coil weighting factors may also be used to improve the quality of the resulting PDw images by reconstructing them using Eq. (15) with the smoothed (low resolution) estimates instead of the original estimates of the coil weighting factors, as was proposed in Ref. [33].

The resulting T2w image may be calculated as a magnitude of Eq. (18). However, when complex MR images have low SNR, the magnitude operation results in reduced contrast, which obscures low-intensity signals in the noise and creates noise bias. These effects become critical for low SNR images and images in which the MR signal of a specific tissue is suppressed to improve the diagnostic value of the scan (e.g., black-blood angiography). It is advantageous to use a real reconstruction with appropriate phase correction rather than magnitude reconstruction in such cases [30]. Therefore, to decrease the noise bias and improve detectability of low-intensity objects, the resulting T2w image is finally reconstructed by taking the real part from Eq. (18). The real image reconstruction is feasible because individual coil T2w images in Eq. (18) are phase corrected by the phase of the corresponding PDw images.

The third step of the NRR scheme is completely independent of the first two and may be used separately to improve the quality of images acquired by phased array coils. The degree of image improvement (noise bias suppression and contrast enhancement in low SNR image areas) that can be achieved by enacting this step of the noise reduction scheme strongly depends on the noise level in the coil weighing factors and the correlations between the noise in individual coil images and the noise in the corresponding coil weighting factors. The optimal result is attained when the coil weighting factors have high SNR and the noise contributions are completely uncorrelated, such as in the case of reconstruction of T2w images using the coil weighting factors calculated using the corresponding PDw images.

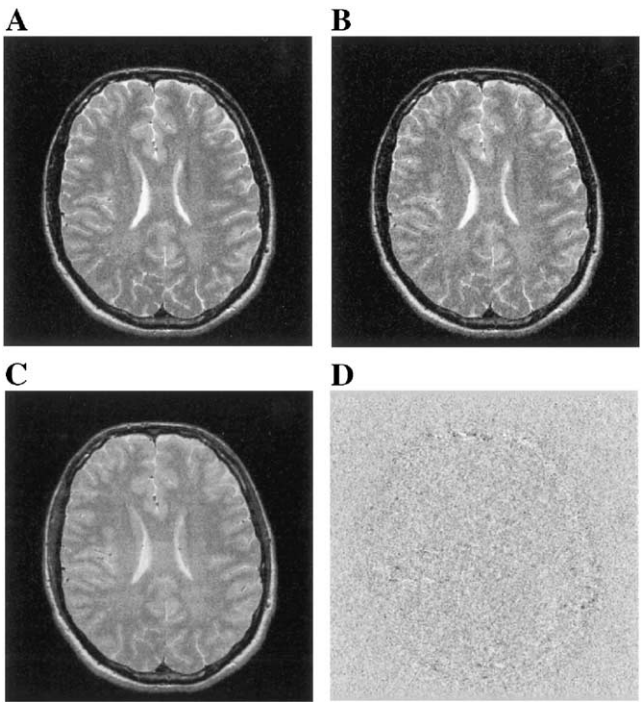

Fig. 4. The T2w brain image reconstructed using (A) complete k-space data, (B) partial k-space data (half k-space plus two more central lines) and five-iterations of a POCS reconstruction with the phase of the corresponding PDw image as a phase constraint. (C) The initial estimate for a POCS reconstruction. (D) The difference between the complete k-space image (A) and the partial k-space image (B). The same color table is used to present images (A–C).

2.3. Imaging experiments

The proposed methods of partial k-space reconstruction and noise reduction were validated by studying their effectiveness on data from a phantom study and human volunteer studies. Informed consent was obtained from all subjects in accordance with our institution's human subjects policies. All imaging studies were performed on a 1.5-T GE SIGNA Lx 8.4 MRI scanner (General Electric Medical Systems, Waukeesha, WI) with NV/CVi gradients (40 mT/m amplitude, 150 mT/m/ms slew rate). Phantom imaging was performed using a custom built four-element bilateral temporal lobe phased array coil. Phantom data were acquired using a dual echo 2D FSE pulse sequence. The imaging sequence parameters were TR=1350 ms, effective TE=7/178 ms for PDw/T2w image acquisition, echo-train length (ETL) of 48, ±62.5 kHz receiver band width (rBW), FOV=240×240 mm^2, 256×256 in-plane acquisition matrix and 2-mm slice thickness. Human subject images were acquired using a dual echo 2D FSE pulse sequence for brain imaging and a black-blood, ECG-gated, dual echo, double inversion recovery FSE pulse sequence [6] for carotid imaging. In brain imaging, a head coil was used and the pulse sequence parameters were TR=3000 ms, effective TE=10/90 ms for PDw/T2w image acquisition, ETL=16, rBW=±20.83 kHz, FOV=220×220 mm^2, 256×256 in-plane acquisition matrix and 2-mm slice thickness. In carotid imaging, the specially designed phased array coils optimized for imaging cervical carotid arteries [35,36] were placed bilaterally on the neck and centered over the region of the bifurcation. Acquisition triggering was performed using the peripheral gate with the inversion pulses occurring at the peripheral pressure pulse (mid to end-systole) and the data acquisition occurring at diastole. This time synchronization allows maximized blood suppression and minimized artifact caused by vessel motion. The imaging sequence parameters were TR=2 RR intervals, effective TE=20/120 ms for PDw/T2w image acquisition, inversion time TI=625 ms, ETL=32, rBW=±62.5 kHz, FOV=140×140 mm^2, 256×256 in-plane acquisition matrix and slice thickness of 2 mm.

Individual coil PDw images were normalized to have the same noise standard deviation. The same normalization factors were applied to the corresponding T2w images. This operation yields improved SNR of the reconstructed images when coils have substantially different noise contributions. After this normalization, the image reconstructed using the SoS algorithm is equivalent to the image reconstructed using the weighted SoS algorithm [37].

Coil weighting factors α_i were estimated based on original and low-resolution PDw images. The low-resolution images were reconstructed using the central part ($Y\times Y$ pixels) of the corresponding k-space data with zeroing of all other k-space data. A Hamming window was used to achieve a smooth transition between zeroed and nonzeroed data. Fig. 3 demonstrates the coil weighting factors calculated using the original PDw, T2w and low-resolution (Y=64) PDw images. All NRR images shown in this paper were reconstructed using all three steps of the NRR method. The NRR black-blood images shown in this paper were reconstructed with Y=64, and the NRR phantom images were reconstructed using high-resolution (Y=256) coil weighting factors.

3. Results

3.1. Improvement of time efficiency

Fig. 4 shows the results obtained using the proposed POCS scheme for reconstruction of highly undersampled (half k-space plus two more central lines from another half) T2w brain data using the phase of the corresponding PDw image as a constraint. The image reconstructed from the combined k-space data set (Eq. (7)) and used as the initial estimate for POCS iterations has clearly mixed (PD–T2w) contrast (Fig. 4C). However, the contrast of the resulting image (Fig. 4B) corresponds to true T2w image contrast, which is apparent in the difference image (Fig. 4D). The difference between the complete k-space image and the POCS reconstructed image is mostly noise, demonstrating the possibility of recovering one echo image from highly undersampled data when the phase estimation is known from the other echo image. The standard partial Fourier

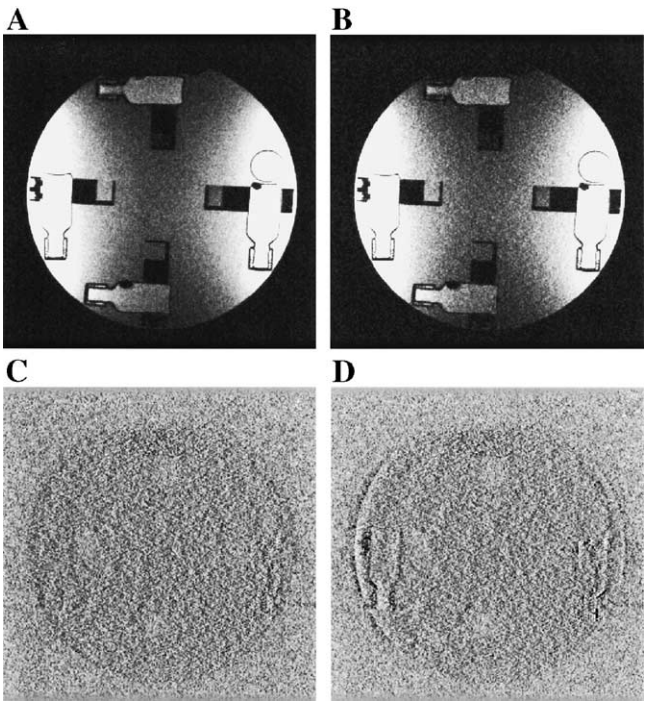

Fig. 5. The SoS T2w phantom image based on the individual coil images that were reconstructed using (A) complete k-space data, (B) partial k-space data (half k-space plus eight more central lines from another half) and four-iterations of POCS reconstruction with the phase of the corresponding PDw image as a phase constraint and an initial estimate calculated from the combination of PDw and T2w k-space data. (C) The difference between the complete k-space image (A) and the partial k-space image (B) is mainly noise. (D) The difference between the complete k-space image (A) and the partial k-space image, which was calculated similar to B, except that the initial estimate was calculated using only acquired T2w k-space data (missing data were zero filled). The correlated features illustrate that convergence of the POCS iterations has not yet been attained.

reconstruction algorithms (homodyne detection, Cuppen, POCS) cannot be used for such high undersampling rates because a few central lines of k-space is not enough to obtain a reasonable estimate of the image phase.

Fig. 5 demonstrates a comparison between the T2w images reconstructed using the SoS algorithm from two sets of individual coil images. The first set consists of the T2w images reconstructed from complete k-space data, while the second set consists of the T2w images reconstructed from partial k-space data using the described POCS reconstruction technique (4 iterations). In the case when the initial estimate for POCS iterations is calculated from the combined T2w and PDw k-space data (Eq. (7)), the difference between the complete k-space image and the POCS reconstructed image is predominantly noise. However, a number of correlated features are quite visible on the other difference image (Fig. 5D), showing that additional iterations are required to achieve convergence when only acquired T2w data are used to find an initial estimate. After two more iterations, the difference between the complete k-space image and the image reconstructed by POCS algorithm with the initial estimate based only on the acquired T2w data looks similar to Fig. 5C. This result confirms that convergence of the proposed POCS reconstruction scheme may be improved when the combined T2w and PDw data are used to calculate the initial estimate.

3.2. Noise reduction

Typical results obtained using SoS (Eq. (8)), MSoS (Eq. (10)) and NRR techniques are shown in Fig. 6. The image reconstructed by MSoS has decreased noise bias and improved contrast in low SNR image areas, relative to the SoS-reconstructed image. However, these improvements are accompanied by a partial destruction of low-intensity objects in the upper part of the image. The noticeable improvements of contrast and low SNR image detail detectability are obvious in the image reconstructed using the proposed NRR scheme. Many details that are completely obscured by noise in the SoS image (Fig. 6A) are clearly visible in the NRR image (Fig. 6C). This difference between the SoS image and the NRR image shows that noise is mostly removed from the background image areas and partially removed from low SNR areas in the NRR image.

The differences between the reconstruction methods are illustrated by the intensity histograms of the images of Fig. 6A, B and C, which are plotted in Fig. 7A and B. A considerable overlap between object and background intensities exists in the SoS-reconstructed image. The overlap is significantly reduced in the MSoS-reconstructed image and almost completely suppressed in the image

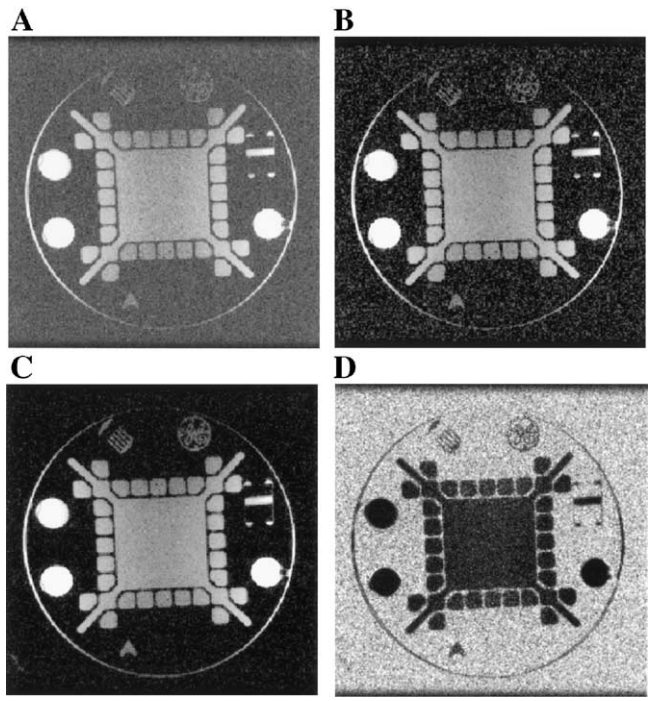

Fig. 6. The T2w phantom image reconstructed using (A) SoS, (B) MSoS and (C) NRR schemes. (D) The difference between A and C shows that the noise was mostly removed from background image areas and partially removed from low SNR areas. The same color table is used to present images (A–C).

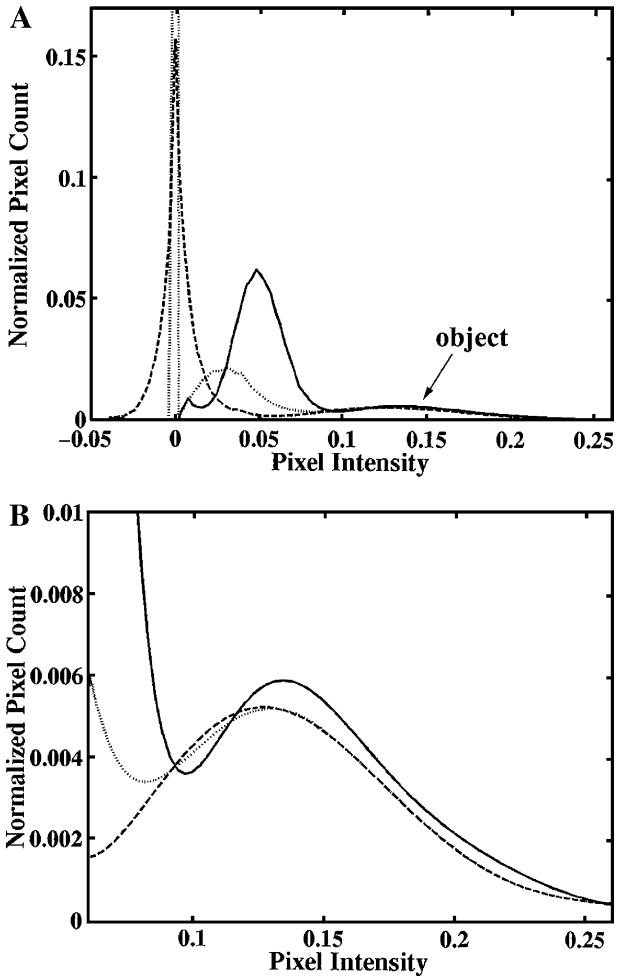

Fig. 7. The histograms of the images shown in Fig. 6A, B and C. (A) The background and object pixel intensity distribution (intensity from −0.05 to 0.26). (B) A zoomed part of A to demonstrate mainly the object pixel intensity distribution (intensity from 0.05 to 0.26). The solid line corresponds to the image reconstructed by SoS (Fig 6A), the dotted line — MSoS (Fig. 6B) and the dashed line — NRR technique (Fig. 6C).

reconstructed using the NRR method. The suppression of the noise bias manifests itself not only as a mean background pixel intensity of zero but also as a shift of object pixel intensity to low values shown in Fig. 7B. The intensity histograms of the MSoS and the NRR images coincide in the medium to high SNR range (Fig. 7B), indicating that the MSoS scheme can be used instead of the NRR method when the low-intensity image areas have no diagnostic value and the true (unbiased) image intensity is desired instead.

Table 1 gives the comparison between different reconstruction methods with respect to the mean value and the standard deviation of the background pixel intensities. Four hundred background pixels of the phantom image shown in Fig. 6 were used for these comparison measurements. In the case of the PDw image reconstruction, the mean value of the background pixel intensity of the resulting image decreases with reduction in the resolution of the PDw coil images used to estimate

Table 1
Mean value and the standard deviation of background pixels

Reconstruction Method	PDw		T2w	
	Mean	σ	Mean	σ
SoS	0.0512	0.0130	0.0513	0.0129
MSoS	0.0135	0.0189	0.0137	0.0189
NRR3 (256)	0.0512	0.0130	0.0005	0.0186
NRR3 (128)	0.0194	0.0171	0.0001	0.0191
NRR3 (64)	0.0103	0.0179	−0.0004	0.0188
NRR3 (32)	0.0051	0.0185	−0.0006	0.0187
NRR (256)	–	–	0.0026	0.0148
NRR (128)	–	–	0.0005	0.0110
NRR (64)	–	–	−0.0001	0.0106
NRR (32)	–	–	−0.0003	0.0106

NRR3—the third step of NRR;(Y)—resolution of PDw images used to calculate coil weighting factors.

coil weighted factors. This result supports the suggestion that effectiveness of the last step of the NRR scheme is proportional to the degree of correlation between the noise contributions in individual coil images and the corresponding coil weighting factors. In the case of the T2w image, the last step of the NRR scheme results in a background pixel mean of zero, independent of the resolution of individual coil PDw images used to obtain the coil weighting factors. The reconstructed image is further improved by reducing the standard deviation of the background after all steps of the NRR scheme have been implemented.

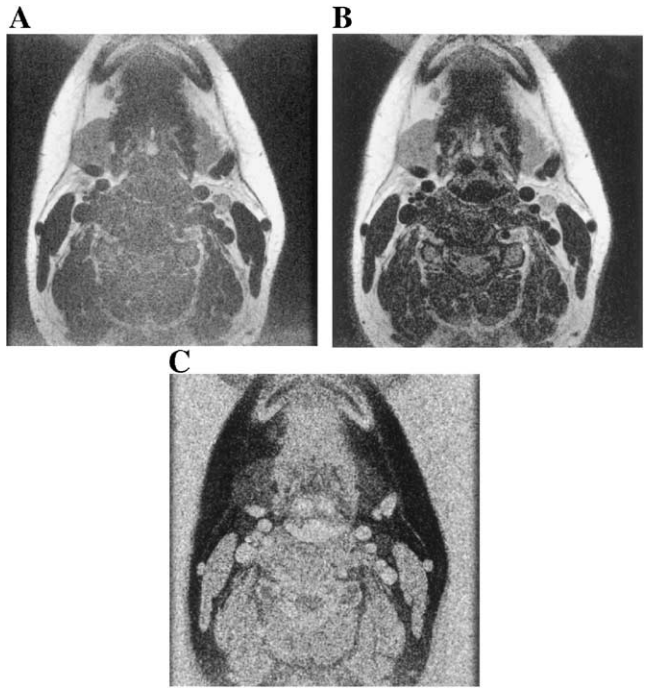

Fig. 8. The T2w images of a volunteer's neck acquired using a dual echo, double inversion FSE sequence. (A) SoS reconstruction, (B) NRR reconstruction. Images A and B were corrected to partially compensate for coil sensitivity inhomogeneity. The same correction function was used for both images. C is the difference between A and B calculated before intensity correction. The same color table is used to present the images A and B.

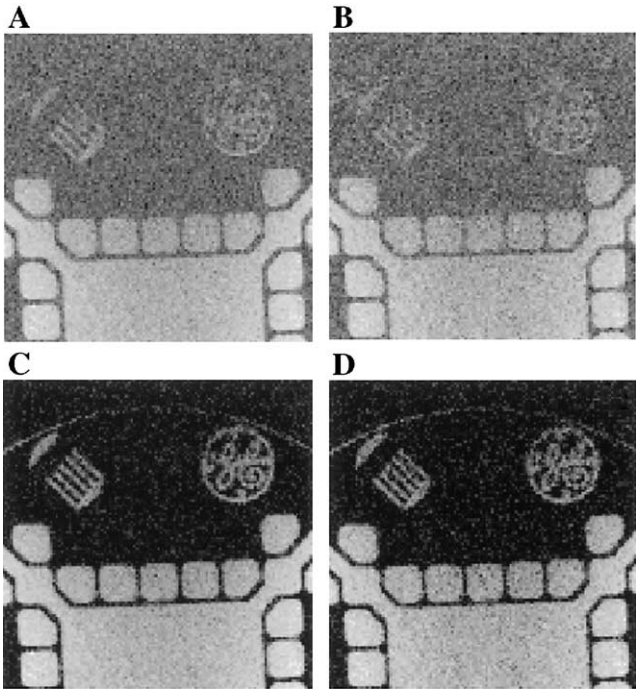

Fig. 9. The zoomed area of the T2w phantom image reconstructed using (A) the SoS method with individual coil images calculated from complete k-space data; (B) the SoS method with individual coil images calculated from partial k-space data (half k-space plus eight central more lines from another half) using the proposed POCS reconstruction scheme (four iterations); (C) the NRR method with the same individual coil images as in A; and (D) the NRR method with the same individual coil images as in B. The same color table is used to present the images.

Fig. 8 shows that the NRR technique improves the T2w image quality in the case of dual echo black-blood angiography. The NRR technique significantly suppresses the noise bias and improves the contrast between lumen and vessel walls. The difference between the original and noise-reduced images shows that most of the noise reduction occurs in regions with no MR signal (background, vessel lumens). However, some noise is removed from regions of low signal.

Fig. 9 demonstrates results obtained from the combined application of both proposed techniques (POCS reconstruction to calculate individual coil images and NRR to optimally combine them) to phantom data. The image reconstructed from full k-space data using the SoS method (Fig. 9A) has a high noise level, which obscures low-intensity objects. The image in Fig. 9B was reconstructed, using the SoS technique, from individual coil T2w images recovered by the POCS technique from partial data. The image has an increased noise level that further degrades visibility of many significant image details. However, when the individual coil images reconstructed from partial data are combined using the NRR method, the resulting image has improved contrast and better low-intensity object detectability than the corresponding T2w image reconstructed from complete data using the SoS method alone.

The noise bias from the SoS method degrades the quality of black-blood angiograms, giving a nonzero mean in vessel areas where the blood signal was completely suppressed and decreasing contrast between the lumen and the vessel wall. Black-blood T2w images of the carotid arteries are shown in Fig. 10. Both SoS-reconstructed images are seriously degraded. The NRR method provides considerably improved visibility of low-intensity image details in areas such as the vessel walls. The NRR images have considerably decreased noise bias and improved contrast. Notice that the T2w image reconstructed from partial data using the

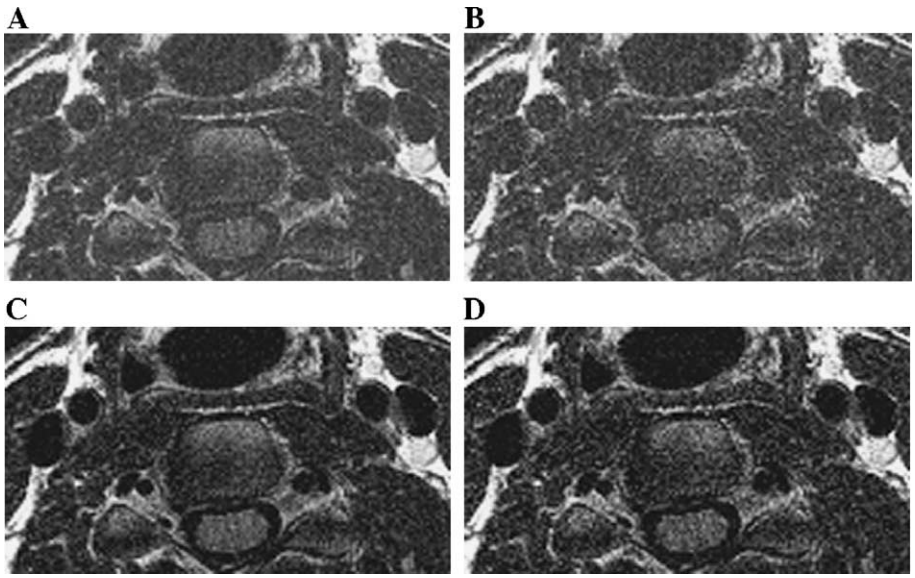

Fig. 10. The zoomed area of the T2w images of the carotid arteries reconstructed using (A) the SoS method with individual coil images calculated from complete k-space data; (B) the SoS method with individual coil images calculated from partial k-space data (half k-space plus eight more central lines from another half) using the proposed POCS reconstruction scheme (four iterations); (C) the NRR method with the same individual coil images as in A; and (D) the NRR method with the same individual coil images as in B. The same color table is used to present the images.

Table 2
Mean value and the standard deviation of vessel lumens pixels

Reconstruction method	PDw		T2w	
	Mean	σ	Mean	σ
SoS	0.0604	0.0171	0.0551	0.0147
MSoS	0.0240	0.0259	0.0161	0.0215
NRR3 (256)	0.0604	0.0171	0.0017	0.0215
NRR3 (128)	0.0147	0.0281	0.0011	0.0216
NRR3 (64)	−0.0081	0.0301	0.0008	0.0217
NRR3 (32)	−0.0107	0.0302	0.0006	0.0221
NRR (256)	–	–	0.0045	0.0173
NRR (128)	–	–	0.0017	0.0143
NRR (64)	–	–	0.0007	0.0144
NRR (32)	–	–	0.0006	0.0146

combined application of both proposed techniques (POCS reconstruction to calculate individual coil images and NRR to optimally combine them) has better diagnostic quality (vessel delineation, contrast between lumen and vessel wall) than the SoS image reconstructed from complete data. Combined application of the proposed techniques allows acquisition of dual echo black-blood angiograms with decreased scan time while maintaining, or improving, diagnostic quality.

Table 2 shows that the NRR scheme yields suppressed noise bias in the vessel lumens (which is obvious in the T2w image results) and displays the true intensity of vessel lumens in the case of PDw image reconstruction using low-resolution coil weighting factors. Three hundred sixty vessel lumen pixels of the image shown in Fig. 10 were used in this experiment. The negative mean of the PDw vessel lumen pixels arose because the double inversion technique was used to suppress the blood signal, and the image acquisition may have started before the inverted blood magnetization attained the T1 relaxation null point, and was therefore still of negative amplitude. Therefore, the last step of the NRR scheme may be used not only to suppress the noise bias and improve contrast in low-intensity image areas, but also to achieve double contrast (negative intensity of vessel lumen and positive intensity of vessel wall) in double inversion black-blood angiograms.

4. Discussion

The phase variations in the PDw and T2w images acquired by the dual echo FSE sequence are the same even though the image contrast may be significantly different. This redundant information may be used to decrease scan time or to optimize image reconstruction in the case of multicoil acquisition. Application of the phase consistency between PDw and T2w images for improved time efficiency and image quality of dual echo black-blood carotid angiography has been considered.

One of the two echo time images might be obtained with greatly reduced k-space coverage by incorporating an estimate of the image phase from the other fully sampled image in reconstruction of the undersampled image. In this manner, the total scan time for dual echo FSE acquisition might be reduced by as much as 25%. Usually, it is preferable to use a phase estimation from the PDw image to reconstruct the T2w image because of the considerably lower SNR of the T2w image. One of the advantages of the proposed scheme is the potential to reconstruct high-quality images from much more undersampled k-space data than is possible with the other partial Fourier reconstruction algorithms. The time-efficiency of dual echo scans can be further improved when a partial acquisition is used to acquire both echo images. In this case, it is preferable to use different undersampling rates (lower for PDw and higher for T2w data) and acquire only partially overlapped k-space areas.

Phased array coils are typically used to acquire dual echo black-blood carotid angiograms. The main purpose of using phased array coils is to distribute the high SNR performance of their small coil elements over a large image area. This reduces the noise contribution from each coil and significantly increases the SNR of the resulting image. However, the images reconstructed by the standard SoS algorithm from the data acquired by phased array coils have increased noise bias in low-intensity areas of the images. In most MRI studies, this effect is completely acceptable. Nevertheless, the existence of the noise bias has a serious detrimental influence on the quality of black-blood images, especially those with strong T2-weighting, giving a nonzero mean in vessel lumen areas where blood signal is completely suppressed and considerably deteriorating contrast between the lumen and the vessel wall. In this study, the NRR technique, which suppresses the noise bias and improves contrast and detectability of low-intensity regions, was developed and tested for phased array coils acquired data. The NRR technique is based on the correspondence between PDw and T2w image intensities and the consistency between PDw and T2w image phases. The primary application of the NRR technique is optimized reconstruction of T2w images acquired by dual echo black-blood acquisitions.

As we have found, the NRR technique works quite well in dual echo black-blood carotid angiography but has not been tested on black-blood angiograms of other vessels. In the case of dual echo black-blood carotid angiography, it is preferable to use coil weighting factors based on low-resolution PDw images rather than on the original PDw images. Both high and low-resolution coil weighting factors give nearly zero mean signal with similar standard deviation in the background of T2w images. However, low-resolution coil weighted factors may be used to further improve the quality of PDw images, as was proposed by Bydder et al. [33]. Additionally, contrast between the lumen and the vessel walls may be doubled when low-resolution coil weighting factors are used. We should note that image improvements, such as the noise bias suppression, and contrast improvement in low SNR image areas are greater for T2w images than they are for the corresponding PDw

images, because the noise in PDw coil images and the noise in the corresponding coil weighting factors are correlated.

Acknowledgments

This work is supported in part by NIH grants R01 HL57990, R01 HL48223 and R01 HL53596.

References

[1] Edelman RR, Chien D, Kim D. Fast selective black blood MR imaging. Radiology 1991;181:655–60.
[2] Liu Y, Riederer SJ, Ehman RL. Magnetization-prepared cardiac imaging using gradient echo acquisition. Magn Reson Med 1993; 30:271–5.
[3] Simonetti OP, Finn JP, White RD, Laub G, Henry DA. "Black blood" T2-weighted inversion-recovery MR imaging of the heart. Radiology 1996;199:49–57.
[4] Fayad ZA, Fuster V, Fallon JT, Jayasundera T, Worthley SG, Helft G, et al. Noninvasive in vivo human coronary artery lumen and wall imaging using black-blood magnetic resonance imaging. Circulation 2000;102:506–10.
[5] Song HK, Wright AC, Wolf RL, Wehrli FW. Multislice double inversion pulse sequence for efficient black-blood MRI. Magn Reson Med 2002;47:616–20.
[6] Parker DL, Goodrich KC, Masiker M, Tsuruda JS, Katzman GL. Improved efficiency in double-inversion fast spin-echo imaging. Magn Reson Med 2002;47:1017–21.
[7] Yarnykh VL, Yuan C. Multislice double inversion-recovery black-blood imaging with simultaneous slice reinversion. J Magn Reson Imaging 2003;17:478–83.
[8] Kim SE, Kholmovski EG, Jeong EK, Buswell H, Tsuruda JS, Parker DL. Triple contrast technique in black blood imaging using double inversion preparation. Magn Reson Med 2004;52:1379–87.
[9] Martin AJ, Gotlieb AI, Henkelman RM. High-resolution MR imaging of human arteries. J Magn Reson Imaging 1995;5:93–100.
[10] Toussaint JF, LaMuraglia GM, Southern JF, Faster V, Kantor HL. Magnetic resonance images lipid, fibrous, calcified, hemorrhagic, and thrombotic components of human atherosclerosis in vivo. Circulation 1996;94:932–8.
[11] Rogers WJ, Prichard JW, Hu YL, Olson PR, Benckart DH, Kramer CM, et al. Characterization of signal properties in atherosclerotic plaque components by intravascular MRI. Arterioscler Thromb Vasc Biol 2000;20:1824–30.
[12] Higushi N, Oshio K, Momoshima S, Shiga H, Melki PS, Mulkern RV, et al. Two-contrast RARE: a fast spin-density and T2-weighted imaging method. J Magn Reson Imaging 1991;1:147.
[13] Melki PS, Mulkern RV, Panych LP, Jolesz FA. Comparing the FAISE method with conventional dual-echo sequences. J Magn Reson Imaging 1991;1:319–26.
[14] Hinks RS, Echo-sharing. US Patent 5168226, 1992. Available at: http://www.uspto.gov/patft.
[15] Johnson BA, Fram EK, Drayer BP, Dean BL, Keller PJ, Jacobowitz R. Evaluation of shared-view acquisition using repeated echoes (SHARE): a dual-echo fast spin-echo MR technique. AJNR Am J Neuroradiol 1994;15:667–73.
[16] Henkelman RM, Hardy PA, Bishop JE, Poon CS, Plewes DB. Why fat is bright in RARE and fast spin-echo imaging. J Magn Reson Imaging 1992;2:533–40.
[17] Constable RT, Anderson AW, Zhong J, Gore JC. Factors influencing contrast in fast spin-echo MR imaging. Magn Reson Imaging 1992; 10:497–511.
[18] Margosian P, Schmitt F, Purdy D. Faster MR imaging: imaging with half the data. Health Care Instrum 1986;1:195–7.
[19] Cuppen J, van Est A. Reducing MR imaging time by one-sided reconstruction. Magn Reson Imaging 1987;5:526–7.
[20] Noll DC, Nishimura DG, Macovski A. Homodyne detection in magnetic resonance imaging. IEEE Trans Med Imaging 1991; 10:154–63.
[21] Youla DC. Mathematical theory of image restoration by the method of convex projection. In: Stark H, editor. Image recovery: theory and application. Orlando: Academic Press; 1987. p. 29–77.
[22] Haacke EM, Lindskog ED, Lin W. A fast, iterative, partial-Fourier technique capable of local phase recovery. J Magn Reson 1991; 92:126–45.
[23] Liang ZP, Boada FE, Constable RT, Haacke EM, Lauterbur PC, Smith MR. Constrained reconstruction methods in MR imaging. Rev Magn Reson Med 1992;4:67–185.
[24] McGibney G, Smith MR, Nichols ST, Crawley A. Quantitative evaluation of several partial Fourier reconstruction algorithms used in MRI. Magn Reson Med 1993;30:51–9.
[25] Kellman P, Arai AE, McVeigh ER, Aletras AH. Phase-sensitive inversion recovery for detecting myocardial infarction using gadolinium-delayed hyperenhancement. Magn Reson Med 2002; 47:372–83.
[26] Hua J, Hurst GC, Duerk JL. Some noise properties of 2DFT MR images from asymmetrically sampled data. Med Phys 1992; 19:1191–4.
[27] Constantinides CD, Atalar E, McVeigh ER. Signal-to-noise measurements in magnitude images from NMR phased arrays. Magn Reson Med 1997;38:852–7.
[28] Roemer PB, Edelstein WA, Hayes CE, Souza SP, Mueller OM. The NMR phased array. Magn Reson Med 1990;16:192–225.
[29] Henkelman RM. Measurement of signal intensities in the presence of noise in MR images. Med Phys 1985;12:232–3 [erratum in Med Phys 1986; 13:544.
[30] Bernstein MA, Thomasson DM, Perman WH. Improved detectability in low signal-to-noise ratio magnetic resonance images by means of a phase-corrected real reconstruction. Med Phys 1989; 16:813–7.
[31] McGibney G, Smith MR. An unbiased signal-to-noise ratio measure for magnetic resonance images. Med Phys 1993;20:1077–8.
[32] Miller AJ, Joseph PM. The use of power images to perform quantitative analysis on low SNR MR images. Magn Reson Imaging 1993;11:1051–6.
[33] Bydder M, Larkman DJ, Hajnal JV. Combination of signals from array coils using image-based estimation of coil sensitivity profiles. Magn Reson Med 2002;47:539–48.
[34] Hua J, Hurst GC. Noise and artifact comparison for Fourier and polynomial phase correction used with Fourier reconstruction of asymmetric data sets. J Magn Reson Imaging 1992;2:347–53.
[35] Hayes C, Mathis C, Yuan C. Surface coil phased arrays for high-resolution imaging of the carotid arteries. J Magn Reson Imaging 1996;6:109–12.
[36] Hadley JR, Chapman BE, Roberts JA, Chapman DC, Goodrich KC, Buswell HR, et al. A three-coil comparison for MR angiography. J Magn Reson Imaging 2000;11:458–68.
[37] Bernstein MA, Grgic M, Brosnan TJ, Pelc NJ. Reconstructions of phase contrast, phased array multicoil data. Magn Reson Med 1994;32:330–4.